

Robust GNSS Shadow Matching for Smartphones in Urban Canyons

Hoi-Fung Ng, Guohao Zhang, *Student Member, IEEE*, and Li-Ta Hsu, *Member, IEEE*

Abstract— GNSS is being widely used in different applications in navigation. However, GNSS positioning is greatly challenged by notorious multipath effects and non-line-of-sight (NLOS) receptions. The signal blockage and reflection by buildings cause these effects. In other words, the more urbanized the city is, the more challenge on the GNSS positioning. The conventional multipath mitigation approaches, such as the sophisticated design of GNSS receiver correlator, can efficiently mitigate the most of multipath effects. However, it has less capability against NLOS reception, potentially leading to several tens of positioning errors. Therefore, the 3D mapping aided (3DMA) GNSS positioning is introduced to exclude or even use the NLOS signal. Shadow matching is to make use of the similarity between building geometry and satellite visibility to improve the positioning performance. This paper introduces a machine learning intelligent classifier with features to distinguish LOS and NLOS. With the NLOS reception classification, the positioning accuracy of shadow matching can be increased. In addition, this paper develops several indicators to label the unreliable solution of shadow matching. These indicators are to examine the complexity of the surrounding environment, which is the key factor relating to the proposed shadow matching performance. Several designed experiments were done in Hong Kong to evaluate the proposed method. With the intelligent classifier, the average positioning accuracy is about 15m and 6m on 2D and the across-street direction, respectively. Simultaneously, the reliability evaluation rules can exclude unreliable epoch and improve the positioning results, especially on smartphone data.

Index Terms—GNSS, Navigation, Smartphone, 3D building model, Urban canyons, Multipath and NLOS

I. INTRODUCTION

GNSS is widely adopted in different location-based-service (LBS) [1]. Users always want to have high positioning accuracy, especially for those low-cost receivers, and the performance of LBS tightly relies on it. However, the urban area is still a challenging environment for the majority of the low-cost GNSS receivers and smartphone users and suffering dozens of meter positioning errors [2, 3]. The positioning error comes from the GNSS signal blockage or reflection by the building surface, namely multipath and NLOS signals [4]. These errors are common in deep urban canyons and results in the extra travelling distance for the signal, which introduces a large positioning error for more than 50 meters [5].

As the conventional single point positioning algorithm, weighted least-squares still suffers from several ten meters of positioning error. The differential Global Navigation Satellite System (DGNSS) correction can significantly reduce the positioning error in the open-sky area, but not for the urban one. Different researches are trying to mitigate the NLOS reception to improve positioning accuracy. The consistency-check method [6] can detect and exclude those unhealthy measurements to obtain better positioning accuracy. However, in the dense urban area, multiple NLOS reception may lead to fault consistency issue and degrade the correctness of fault detection and exclusion [7].

Researches also proposed improving urban positioning by extra equipment, which is suitable for vehicle-mounted applications. [8, 9] proposed using the sky-pointing fisheye camera to exclude the NLOS satellites by image recognition. Another approach is using the 3D light detection and ranging (LiDAR) to provide surrounding environment obstacles and

detect the NLOS signal [10]. NLOS propagation model can calculate the pseudorange correction based on the distance to the building provided by LiDAR [11]. By integrating with the sky-pointing fisheye camera with LiDAR, the positioning accuracy in urban areas can be improved [12]. The NLOS classified satellite can be excluded or de-weighted to provide a more reliable GNSS position solution.

With the trend on 3D building model resources become more common worldwide for open access. For example, the 3D building model can be made by combining the satellite images and airborne LiDAR, where the former and latter ones provide 2D building contour and building height, respectively [13]. A complete review of the making of large-scale 3D building models can be found at [14]. These 3D models provide the opportunity to make use of the model to improve the performance, which is well-known as the 3D mapping aided (3DMA) GNSS [15]. The 3DMA GNSS positioning algorithms as NLOS-excluded positioning [16], shadow matching [17, 18], likelihood-based 3DMA GNSS [19], ray-tracing 3DMA GNSS [20, 21], and skymask 3DMA GNSS [22]. The shadow matching, proposed by [18], uses the building boundaries from the 3D city model and compare the satellite visibility similarity between the actual received signal to determine user position. Due to the similarity of the building geometry, shadow matching usually performs better on the across street direction [23]. Therefore, the likelihood-based 3DMA GNSS was introduced to use the measurements on the along-street direction. The integration solution on the shadow matching and likelihood-based 3DMA GNSS to improve both along and across street accuracy was introduced by [19]. The ray-tracing-based 3DMA GNSS positioning provides a more intensive purpose for detecting and correcting the reflected signal on

NLOS reception. The ray-tracing traces the possible transmission route of both direct and reflected GNSS signals based on 3D building models. Therefore, the measurement delay distance due to the reflection can be provided to correct the pseudorange.

Under the shadow matching assumption, the received satellite with the C/N_0 larger than a threshold is assumed to be the LOS satellite, e.g., 35 dB-Hz [23]. On the other hand, for those satellites are not received, the building should block them. Therefore, compare to all candidates, near the ground truth, one should obtain the highest similarity between the LOS and NLOS reception and prediction by building geometry. However, the signal can be reflected by or penetrated through the building and received, which results in NLOS reception. The NLOS reception will accidentally identify the satellite is the LOS one and affect the scoring for the agreement between geometry. To mitigate the NLOS reception effect, researchers are proposed to use the machine learning model to classify the received signal [24-26] and exclude those NLOS reception satellites from scoring.

In this paper, the shadow matching will be analyzed. This paper has two main contributions: 1) adopting the machine learning classifier to classify out the NLOS reception and improve the shadow matching performance. 2) introducing the reliability evaluation scheme of shadow matching performance. The scheme aims to let users know whether the shadow matching is functional at the environment and the confidence of the position solution, whether it is trustworthy. Total four rules are introduced and used to evaluate whether the single point solution estimated by the shadow matching is reliable.

The positioning accuracy and reliability will be evaluated by experiments conducted in urban canyons of Hong Kong. The across-street accuracy can achieve within 10m. With the reliability exclusion, the positioning accuracy can further improve in both across- and along-street direction.

The paper is organized as follows. An overview of shadow matching will be done in Section II. The reliability evaluation scheme of shadow matching is presented in Section III. The experimental results on intelligent classifier accuracy and positioning are given in Section IV. Finally, the conclusions and future work are given in Section V.

II. OVERVIEW OF SHADOW MATCHING

A. Skymask Generation

The ‘skymask’ is the building boundary projected on the skyplot with a given position.

The offline process does the skymask generation process at the server-side, the whole process to generate skymask for one location is identical to the study proposed in [22]. The skymask of each candidate location is generated with the 3D city model. Thus, the skymask can be initially stored in the device. Based on the 3D building model or in storage perspective, a specific area is selected and divided into grid points to construct the skymask table. The grid point separation is set to 2 meters to generate the skymask. The generation process assumes the user (receiver) always stays on the ground (mean-sea-level). Therefore, the height of the skymask position used in this paper is given by the mean-sea-level datum by the Hong Kong Lands

Department [27].

Fig. 1 is an example of the generated skymask and storage format. The azimuth is in 1-degree resolution, and the elevation is in 0.1-degree resolution. The azimuth angle starts from the north direction, rotating in the clockwise direction; the elevation angle starts from the horizon as 0° .

Azimuth (degree)	Elevation (degree)
1	41.8
2	41.3
3	40.9
...	...
359	42.7
360	42.3

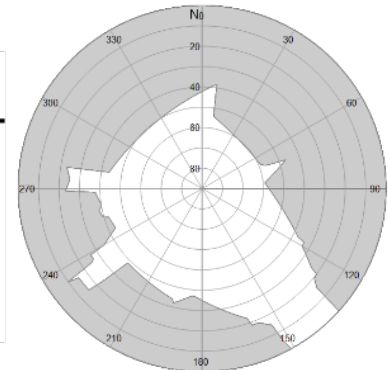


Fig. 1. The data format of the skymask (left) and visualization (right). If the satellite elevation is lower than the building boundary elevation (under the same azimuth angle), it is assumed to be an NLOS signal blocked by buildings.

Each location will first determine whether it is inside a building. For the outside building location, a list of total 360-degree will be used to store the maximum elevation angle of building edge for corresponding azimuth angle; for the ‘inside building’ location, a flag will be given to represent this location is inside building. The offline generation at the server side is more effective for a low-cost device with limited computational power in practical application.

B. Satellites Visibility Estimation

The shadow matching's main contribution is to determine user position based on the satellite visibility by comparing the satellite visibility between geometry-based and received signal-based determination. In the geometry-based determination, the corresponding skymask will be extracted from the pre-computed skymask table with the given location. The satellite position is estimated using the ephemeris data, which is used to calculate the relative satellite angular position and express in azimuth and elevation angles. The angular position is then put on the skymask. If the elevation angle of the satellite is larger than that of the skymask at corresponding azimuth, it is a LOS satellite, otherwise, it is a NLOS satellite.

Fig. 2, it should be blocked and not received as the red path shown, but the signal is coming in with the blue reflected path. If we consider these signals is the LOS one, there will be a contradiction between skymask prediction and received signal.

The features of the satellite signal on C/N_0 , elevation angle,

pseudorange residual, and pseudorange rate residual will be used to predict the received satellite is either LOS or NLOS. The dataset is trained by the linear support vector machine (SVM) as it has better generalization performance than the decision tree and kNN because the SVM can prevent overfitting problem. The training data cover different urban environment to ensure different natures of signals are included in the classifier model. The LOS/NLOS labelling is done by skymask visibility estimation at ground truth and utilized the SVM function in Matlab for training the intelligent classifier.

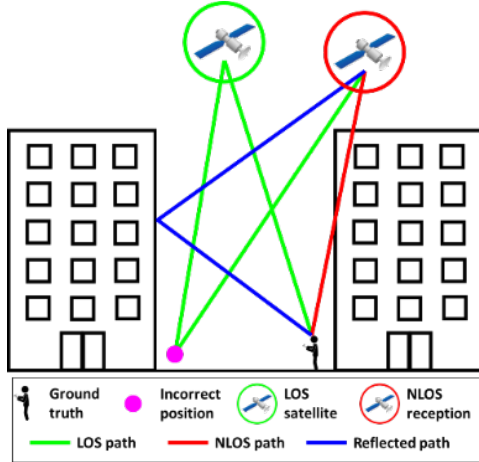


Fig. 2. Example of NLOS reception affecting GNSS shadow matching. Both locations on the opposite side of the street can receive both satellites, which may degrade the shadow matching performance.

C. Position Determination

The shadow matching idea is to compare the similarity between the geometry and signal on each selected position candidates, and the highest similarity will be chosen to be the solution. The overall flowchart for the proposed GNSS shadow matching is shown in Fig. 3.

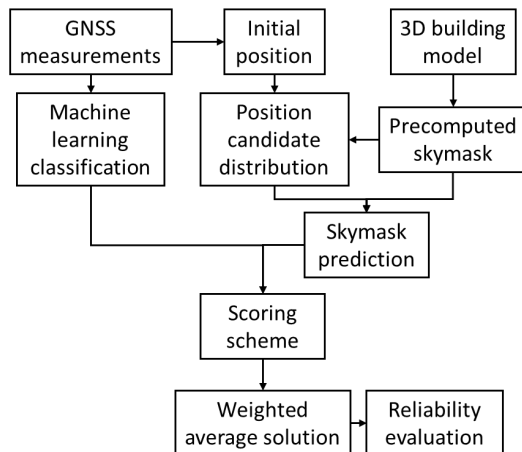


Fig. 3. Flowchart of the proposed GNSS shadow matching.

The received signals will first be fed into the intelligent classifier. The NLOS reception classified signal will consider as the NLOS one to compare with the satellite visibility determined by 3D building models. As mention in section II.B, the intelligent classifier should classify those received NLOS satellites. The NLOS reception will degrade the shadow

matching performance, and the score at the incorrect position will be higher than or similar to that at ground truth, as shown in Fig. 2. Both ground truth and incorrect position are located on the opposite side of the street, but they can receive both satellites. However, the NLOS received satellite (red circled satellite) should not be received intentionally. It should be classified as NLOS by skymask, and this will result in the incorrect position obtains a higher similarity than that of ground truth. As a result, an intelligent classifier is needed and consider the unhealthy measurements as NLOS one in the scoring scheme.

Meanwhile, several position candidates will first be distributed around the initial position, and only the candidates located outside the building are selected. The initial position is important to the positioning hypothesis-based method. The candidate distribution should cover the receiver truth location to estimate the correct satellite visibility, or the sampling radius need to be enlarged either. In this paper, the initial position is the NMEA solution given by commercial GNSS receivers or smartphones. The candidates will be distributed in a circle grid with a 40m radius and 2m separation. In our experience, the positioning uncertainty of NMEA is within 20m in most of the case. Therefore, with candidates sampling radius of 40m, candidates are able to cover and estimate the truth location in order to get the best accuracy. The position candidate sampling size can be varied based on the quality of the initial position, such as least-squares residual [19].

Then, the LOS/NLOS prediction by skymask will be performed at each candidate. All satellites from ephemeris are labelled on the skymask and classified as LOS and NLOS as the skymask classification results. A score is then given to the candidate based on the agreement between the skymask prediction and intelligent classifier results. The score of the i -th satellite at j -th candidate notated as s_j^i , is given in Table I.

TABLE I
TRUTH TABLE FOR SATELLITE SCORING AT THE CANDIDATE

		Received and intelligent classifier result		Not received
		LOS	NLOS	
Skymask classification	LOS	1	0	0
	NLOS	0	1	1

After scoring all satellites for the candidate, the sum of the score will be the score for the candidate, τ_j .

$$\tau_j = \sum s_j^i \quad (1)$$

Then, the candidates' score will be normalized. The top 5% of the candidates with the highest score will be chosen to calculate the solution. The solution x is calculated by the weighted average of the selected 5% candidates with the highest score, $\Lambda \in$ highest 5% of $\{\tau_1 \dots \tau_j\}$.

$$x = \frac{\sum \Lambda P}{\sum \Lambda} \quad (2)$$

Where the Λ denotes the score of the selected candidates, and P is the position of the chosen candidates with the highest 5% score.

III. RELIABILITY EVALUATION

The evaluation of the safeness in using the GNSS shadow matching is very challenging, statistically. Our proposed approach plays a role in selecting the shadow matching solutions that fulfil the rules (derived based on the theory of GNSS shadow matching) of a good estimation. In a real application, the exclusion of unreliable solutions is beneficial for multi-sensor integrated navigation system. Therefore, the reliability evaluation is necessary.

Total of four rules are defined and will be introduced in this section. These evaluations aim to provide indicators to forecast the shadow matching performance. The indicators are designed by the uniqueness of the surrounding building geometry for the satellites matching. For example, shadow matching will not work in an opensky environment as there are not enough features to match with as shown in rule 1 R_1 . Also, the high similarity of building geometry like two parallel streets will result in multiple clusters with high score which will give a high uncertainty to the solution, so we target to find out the multiple clusters and determine the confidence level for the solution as shown in rule 3 R_3 . Another critical point for shadow matching is the satellite distribution to match the building geometry. Therefore, the indicator will consider how the satellite distribution matching with the building geometry as shown in rule 2 R_2 . These indicators are designed for the smartphone and low-cost GNSS receiver to use, where their measurements may be noisier comparing to a geodetic receiver. When these indicators label the shadow matching is not trustable, we can exclude that epoch's solution. Although this will decrease the shadow matching availability, it can provide a more robust positioning solution for the user. The positioning results after solution exclusion based on different reliability rule will be presented in section IV.C.

A. Rule 1 R_1 : Applying Shadow Matching Determine Factor

The first rule is the factor to determine whether the shadow matching is functional. As we know, the shadow matching performs well in urban canyons in the condition that unique building features are sufficient. As the open-sky areas contain very few buildings, the shadow matching is not suitable for such environments. Therefore, this rule is to check whether all the candidates located in an open-sky environment averagely. If most of the candidates are located in an open-sky environment, this indicator will reflect a high value, which is calculated by,

$$R_1 = \frac{\overline{S_{LOS}}}{S} \quad (3)$$

Where $\overline{S_{LOS}}$ is the average number of LOS satellite classified by the skymask classification of all distributed candidate and S is the total number of satellite that its elevation angle is higher than 0 degrees based on the broadcast ephemeris.

Rule 1 can examine whether the distributed candidates' environment is too open for the shadow matching to give a reliable solution. The lower value of the R_1 is, the deeper the urban canyon the receiver is located at, the high reliability of the shadow matching solution is expected.

B. Rule 2 R_2 : Surrounding Features

Rule 2 is to examine the richness of surrounding building features for the shadow matching. The unique structure of surrounding buildings is, the more accurate for the shadow matching solution is.

In here, a concept of 'key satellite' needs to be introduced. The key satellite is the satellite(s) that falls near the building edge, like the cyan and yellow satellites shown in Fig. 4. Based on the shadow matching principle, the satellite distribution is important to match the building boundaries in the skymask. Precisely, satellites fall around the building boundaries are the main features to be matched with skymask and more critical for the shadow matching. Therefore, we offset the skymask on both azimuth and elevation angle, named 'key satellite area' in Fig. 4, and see how many satellites fall inside this area. These satellites inside the offset area well named as 'key satellite'. If a larger number of satellites are labelled as 'key satellite' overall satellite, a higher probability of the best match on this candidate.

When performing the skymask prediction at each candidate, the skymask building edge will offset the azimuth and elevation angle with 10 degrees. For the LOS classified satellites, an extra 5 degrees will be added. If the offset building edge covers the satellite, that satellite will be labelled as the key satellite.

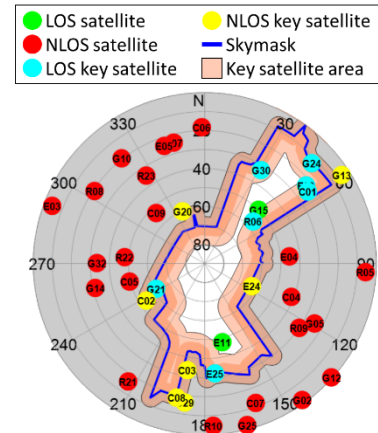


Fig. 4. Illustration of the proposed key satellite classification for GNSS shadow matching. The searching offset angle is 10 degrees for both azimuth and elevation angles. The LOS area will add an extra 5 degrees to search the key satellite.

Rule 2 calculates the number of the classified key satellites in the total number of satellites for the scoring (total number of received satellites and ephemeris satellites) at the solution position.

$$R_2 = \frac{\overline{S_{key}}}{S} \quad (4)$$

The $\overline{S_{key}}$ is the average number of key satellites at highest 5% of the candidate, and S is the total number of visible satellite based on a broadcast ephemeris.

The higher value of rule 2 is, the better performance of shadow matching should be obtained. It means the more features for shadow matching to compare the received satellites

with the classified satellite visibility of candidates based on skymask. Therefore, we can know whether the candidate has the unique features to matching with the satellite visibility.

C. Rule 3 R_3 : Confidence Level at Multiple Cluster

Rule 3 examine the local minima problem on selected candidates with the highest similarity on satellite visibility. The local minima's occurrence due to the high similarity of the surrounding building structure and lack of matching features. For example, at two parallel streets with a similar environment, their skymask will be similar and easily identify a wrong position when matching with the satellites, as shown in Fig. 5(b). In other words, the candidate located at the incorrect position may have identical satellite visibility with that of the ground truth location. Therefore, these local minima result in a low confidence level of the weighted average solution.

The calculation of Rule 3 uses the Euclidean distance to separate the candidates with the highest 5% score into the cluster, 15 meters is set as the threshold distance for clustering in this paper. For example, multiple clusters could be found, such as Fig. 5. If the key satellite appears in more than half of the candidates, that key satellite will be the key satellite for the cluster. Then, for the two clusters, the confidence level of rule 3 is calculated by

$$R_3 = \begin{cases} \operatorname{argmax}_{m,n} \frac{S_{m \cap n} \times 2}{S_m + S_n} & N > 1 \\ 0 & N = 1 \end{cases} \quad (5)$$

where $m, n \in \{1, 2, \dots, N\}; m \neq n$

N is the total number of clusters. S_* is the number of key satellite in the $*$ -th cluster. Therefore, $S_{m \cap n}$ is the number of common key satellite between cluster m and n . The calculation of R_3 will go through all combination of any two clusters if more than two clusters were found, the largest calculated value will be used for the R_3 evaluation. If only one cluster is found, Rule 3 will be given 0 for that epoch, which means all the particle are concentrate and higher confidence is given to the solution.

The meaning of this value is the similarity of two clusters. The clusters can be separated using the highest 5% score candidates based on the distance. If more common key satellites were found, it means other candidates obtain similar satellite visibility which is far away. Therefore, the smaller value means the cluster obtains a higher uniqueness.

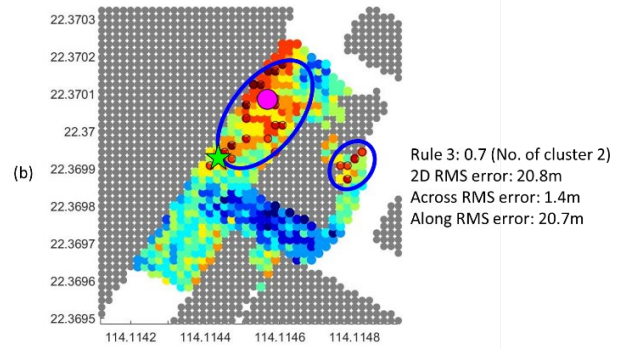
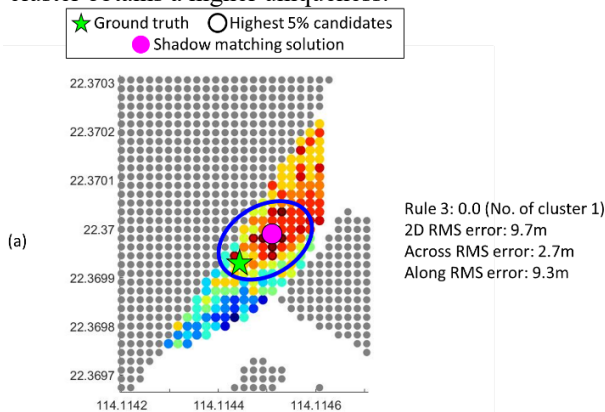


Fig. 5. Illustration of the local minima (two clusters) in GNSS shadow matching. The blue circle is the cluster, the pink point is the shadow matching solution, and the green star is the ground truth. (a) shows the distributed candidates with a single cluster. (b) shows the distributed candidates with multiple clusters.

D. Rule 4 R_4 : Ratio on Achieving Full Score

Rule 4 R_4 is the reliability of shadow matching solution is the ratio of achieving full score. The reliability score is calculated by

$$R_4 = \frac{\bar{\Lambda} - \tau_{\min}}{\tau_{\max} - \tau_{\min}} \quad (6)$$

Where $\bar{\Lambda}$ is the average score of the selected candidates, τ_{\min} and τ_{\max} are the minimum and maximum score of all distributed candidates τ_j , respectively. In here, the higher score of reliability is, the more reliable solution is. R_4 examines how the candidates with the highest 5% score achieve the highest score. The denominator in (6) calculates the range of the score for all distributed candidates. While the numerator is calculating the range of the highest 5% selected candidates to all score. If the average score of selected candidates $\bar{\Lambda}$ are concentrated, and the average value is near the highest score, $\bar{\Lambda} \approx \tau_{\max}$, the R_4 value will fall near to 1. If R_4 near to 1, means solution have a higher possibility to be the optimal solution.

IV. EXPERIMENT RESULTS AND ANALYSIS

A. Experiment Setup and Information

Several experiments were done to evaluate the performance of shadow matching with intelligent classifier. The experiments took place in the urban canyons in Hong Kong. A commercial-grade receiver (Rx1), and two smartphones (Rx2 and Rx3 respectively) were equipped to record the data and post-processing it. The 3D building models are given by the research collaborator, which are in the accuracy of 1-2m. The ground truth is marked on Google Earth manually, and we went to the labelled landmark for the experiments. These ground truth method is following with our previous work in [28].

Table II shows the environments of the experiments. The street width to height ratio is calculated by *mean building height/street width*, the higher value means the area is surrounded by taller building compared to the street width. Namely, the higher value means the higher urbanization of the environment. The environment and

skymask for the experiments are shown in Fig. 6.

TABLE II
EXPERIMENTS INFORMATION

Experiment name	Device	No. of epochs	Experiment type	Street width to height ratio	Half street width (m)
S1-Rx2	Smartphone 1	601	Static	3.07	11.9
S1-Rx3	Smartphone 2	601	Static	3.07	11.9
S2-Rx3	Smartphone 2	421	Static	2.83	12.0
S3-Rx2	Smartphone 1	481	Static	2.47	15.0
S4-Rx1	Commercial	214	Static	2.25	8.0
D1-Rx1	Commercial	69	Dynamic	0.78	32.5
D1-Rx2	Smartphone 1	66	Dynamic	0.78	32.5
D1-Rx3	Smartphone 2	66	Dynamic	0.78	32.5

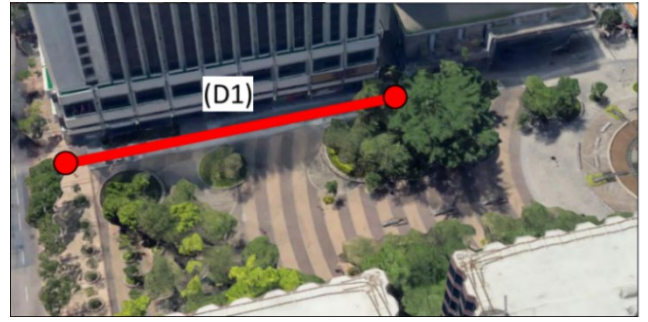


Fig. 6. Environment and skymask of the experiments.

The intelligent classifier model is pre-trained by datasets recorded on different scenarios to ensure the dataset can cover enough signal features [29]. And the experimental data used in this paper did not include in the training datasets.

B. Classification Accuracy and Positioning Results

In this section, the classification rate of intelligent classifier and the positioning results will be evaluated. The positioning results of shadow matching with and without intelligent classifier will be compared.

1) Intelligent Classifier Classification Rate

The overall classification rate is shown in Table III. The LOS and NLOS classification is done at ground truth for each experiment, where the ground truth is labelled manually on Google Earth. The intelligent classifier overall accuracy is about 70%. The feature of the satellite signal on C/N_0 , elevation angle, pseudorange residual, and pseudorange rate residual are used for the NLOS reception exclusion for the intelligent classifier [29].

TABLE III
CLASSIFICATION ACCURACY OF THE EXPERIMENTS

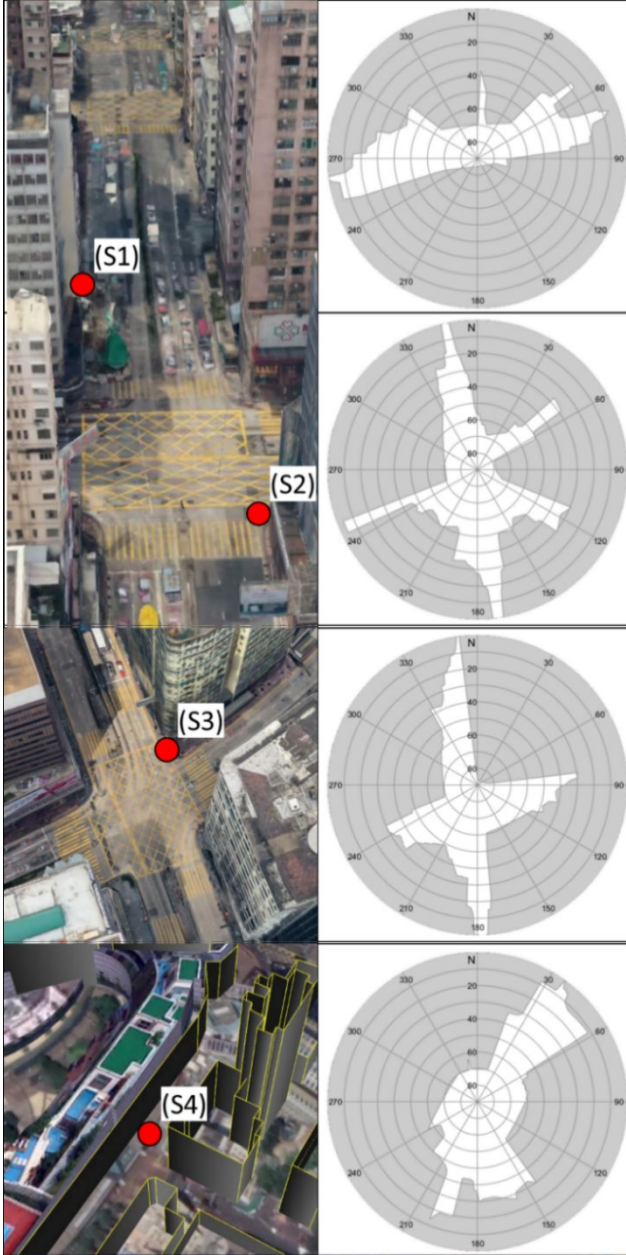
Experiment	Total no. of measurements	No. of measurements correctly classified	No. of measurements incorrectly classified	Overall correctly classified percentage (%)
S1-Rx2	14737	10428	4309	70.76
S1-Rx3	15008	9899	5109	65.96
S2-Rx3	12390	6593	5797	53.21
S3-Rx2	13393	9214	4179	68.80
S4-Rx1	2376	1655	721	69.65
D1-Rx1	1074	888	186	82.68
D1-Rx2	1337	1048	289	78.38
D1-Rx3	1639	1104	535	67.36

2) Positioning Results

The overview on root-mean-square (RMS) error for positioning results is shown in Table IV. The positioning accuracy will be compared with:

1. Weighted-least-squares (WLS), with (42) based on satellites' elevation angle and C/N_0 value [30]
2. Shadow matching without intelligent classifier (SDM)
3. Shadow matching with intelligent classifier (SDM-ML)

The SDM without intelligent classifier only consider the received satellite with C/N_0 larger than 35dBHz as the LOS satellite. While the SDM-ML first extracts the measurement features, then puts into the intelligent classifier to select out the NLOS reception.



The actual datasets determine C/N_0 threshold with 35 dBHz for SDM without the intelligent classifier, shown in Fig. 7. For both smartphone and commercial-grade receiver, the C/N_0 of LOS signal is usually larger than 35 dBHz.

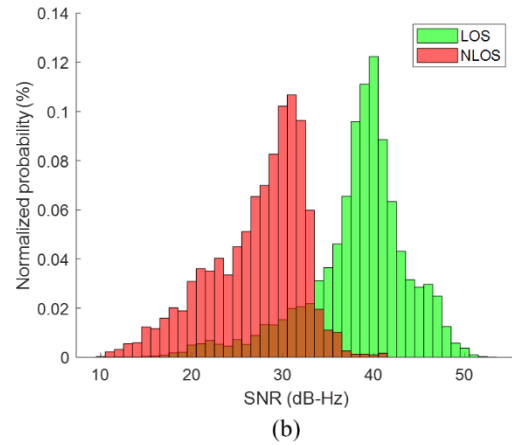
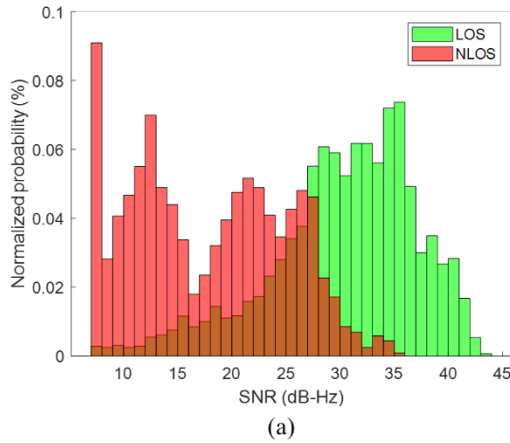


Fig. 7. Normalized SNR distributions of LOS and NLOS signals of (a) smartphone and (b) commercial-grade receiver dataset.

The positioning error will be shown in the 2D direction, which is the displacement between ground truth and solution. The error will also be decomposed into across- and along- street directions. The along-street direction is determined manually based on the building geometry distribution.

TABLE IV
OVERALL EXPERIMENTS POSITIONING ACCURACY (IN METERS)

Experiment	WLS RMS error (m)			SDM RMS error (m)			SDM-ML RMS error (m)			Percentage of SDM-ML epoch within half street width (%)
	2D	Across	Along	2D	Across	Along	2D	Across	Along	
S1-Rx2	22.84	20.39	10.29	17.80	4.23	17.29	7.29	4.11	6.02	100.0
S1-Rx3	147.34	82.89	121.82	24.76	13.49	20.77	7.61	4.21	6.33	100.0
S2-Rx3	110.02	74.21	81.23	22.96	16.09	16.37	17.30	12.71	11.74	60.1
S3-Rx2	22.10	16.03	15.22	40.87	23.78	33.24	40.25	15.27	37.24	54.1
S4-Rx1	39.88	36.61	15.81	14.54	7.72	12.32	17.76	4.86	17.08	97.7
D1-Rx1	37.38	36.45	8.30	39.76	34.04	20.55	10.79	3.01	10.36	100.0
D1-Rx2	40.11	39.58	6.50	28.62	13.55	25.21	10.37	1.93	10.19	100.0
D1-Rx3	112.94	56.79	97.62	27.66	13.12	24.35	13.41	2.26	13.22	100.0

The shadow matching performance can achieve about 5m in across street direction, while the total 2D error most of them can achieve about 10m error. Solutions distribution on the map for the shadow matching with intelligent classifier, as shown below.

The experiment S1 surrounds with aligned building along the street. Therefore, the positioning results are good in the across-

street direction, as shown in Fig. 8. For the experiment S1 with both smartphones Rx2 and Rx3, the across street direction RMS can achieve about 4m. From the distribution of the solutions, the SDM-ML can improve along-street accuracy. And for the S1-Rx3, the across-street direction accuracy improves much.

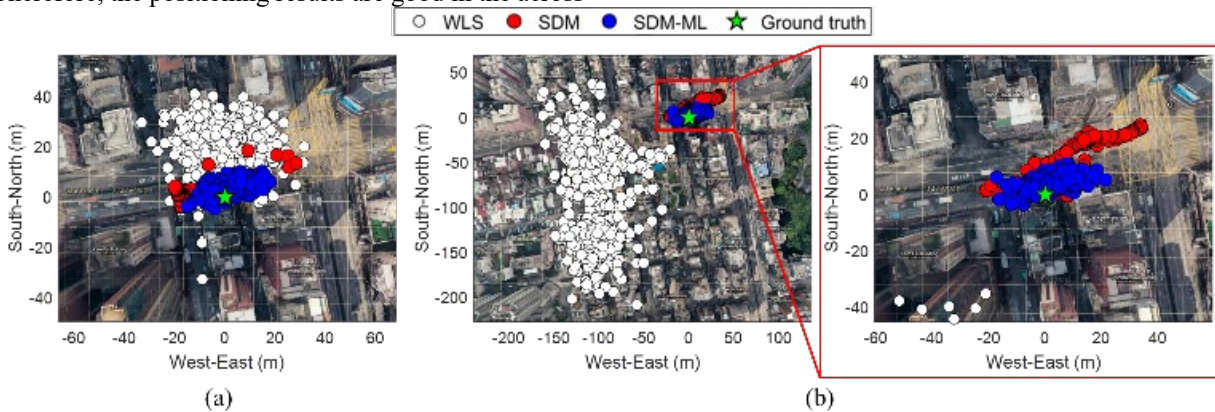


Fig. 8. Positioning results of S1 on (a) Rx2 and (b) Rx3.

Both the experiment S2 and S3 are located at the intersection of the road, where buildings are not aligned and do not have a clear along street direction. In other words, the positioning uncertainty is the same in both along- and across-street

directions. For the S2-Rx3, both the across- and along-street direction errors achieve about 12m. Fig. 9 shows the positioning results of S2-Rx3, where the positioning results of SDM without intelligent classifier, the solutions distribute across the whole intersection. The reflected signal come from different

directions, results in counted as LOS and accidentally high score in the candidate at the opposite side of the street. With the intelligent classifier, the received signal visibility estimation can be improved, resulting in the positioning accuracy improve much, and the solutions become more concentrated to the ground truth.

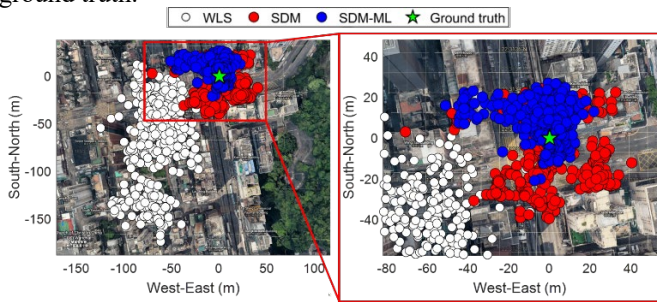


Fig. 9. Positioning results of S2-Rx3.

Furthermore, for the S3-Rx2, the 2D position error achieves 40.25m and 37.24m in the along-street direction, Fig. 10 shows the solution distribution. Similar to S2-Rx3, severe NLOS reception and results in the solution drift to the opposite side of the street. Although intelligent classifier cannot classify all NLOS reception, it still improves the accuracy.

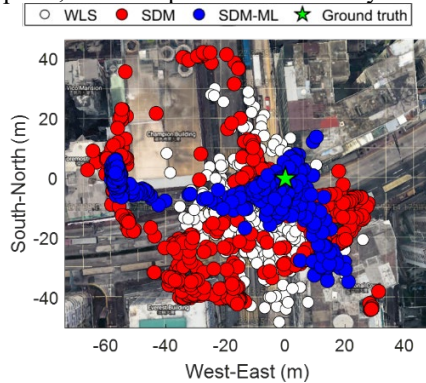


Fig. 10. Positioning results of S3-Rx2.

This considerable error caused by the limitation of shadow matching, the experiment was located in the road intersection. The high similarity of the building from one corner to another cause the error, like the location and corresponding skymasks shown in Fig. 11 (a), (b), and (c) respectively. This high similarity results in the uncertainty for the position candidate's selection, and multiple clusters for the candidates. Cluster near the ground truth obtains a high score of 25, as shown in Fig. 11(b). The score here is identical to the score obtained by father cluster, shown in Fig. 11(c). Although the skymask is different, only a few key satellites to match the skymask to obtain a perfect solution.

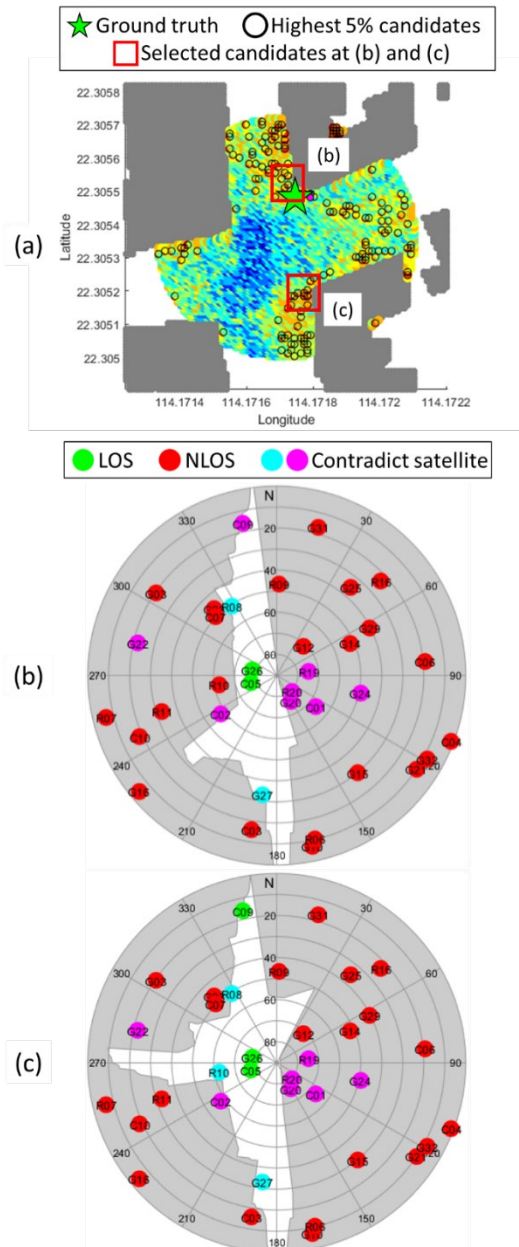


Fig. 11. (a) Position candidates heatmap. (b) Skymask with satellites projected of a candidate at the upper cluster which is near the ground truth. (c) Skymask with satellites projected of a candidate at the lower cluster in (a).

Positioning results of S4-Rx1 are shown in Fig. 12. The positioning accuracy on across-street can achieve within 5m, and the total RMS error is about 18m. However, the along-street error of this experiment is relatively large, which exceeds about 17m. Large positioning error here due to the high similarity of building geometry in the along-street direction. The intelligent classifier improves the across-street accuracy from 8m to 5m. In other words, as the half street width here is 8m, the shadow matching with intelligent classifier can successfully identify the NLOS reception and results in high confident to determine which side of the street is located.

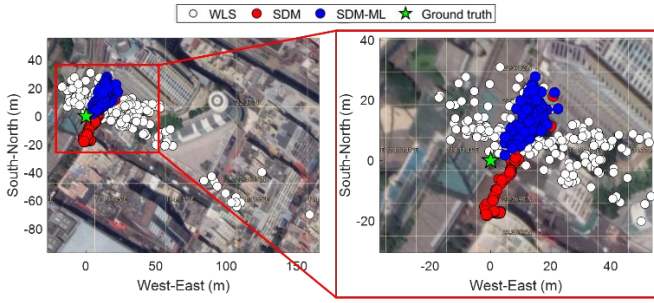


Fig. 12. Positioning results of S4-Rx1.

Experiment D1 locates in a light-urban area, and surrounding buildings are aligned into the same direction. Therefore, all three receivers achieve good positioning results. The positioning accuracy can achieve within 5m in the across-street direction, shown in Fig. 13. The solution of SDM-ML shows that the intelligent classifier can select out those NLOS reception to improve the satellite visibility estimation and the solution sticks near the building side rather than drift towards the middle side.

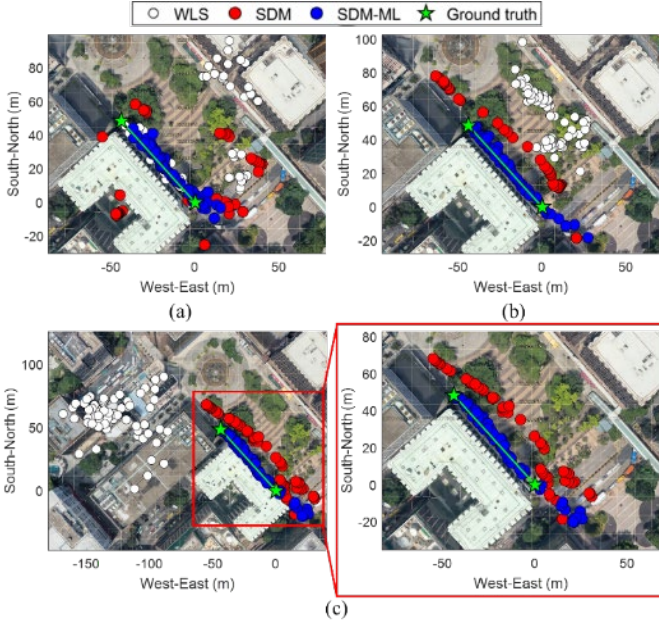


Fig. 13. Positioning results of D1. (a) Experiment D1-Rx1. (b) Experiment D1-Rx2. (c) Experiment D1-Rx3.

C. Reliability Analysis

We use several experiments to improve the reliability indicator performance, we will use the proposed reliability rules to exclude the epoch solution and mitigate the final positioning errors. The passing threshold of the reliability evaluation are given as following. The values are determined heuristically.

- $R_1 < 0.4$
- $R_2 > 0.3$
- $R_3 < 0.5$
- $R_4 > 0.7$

In here, we made a comparison of four main categories. The first is no rule applied as a reference. The second is that only one rule is applied to see the error. The third category is Rule 4 of reliability passed with one other rules. The last one is applying all rules. Also, we combine Rules 1 and 3 to evaluate the performance. We believed that Rules 1 and 3 together could confirm the shadow matching applies on the satisfactory environment, and no multiple clusters or local minimum problem to the selected candidates. Therefore, the solution will be more reliable.

The experiment S2-Rx3 positioning results with reliability evaluation is shown in Table V. The results show that the Rule 2 on the key satellites matching with the skymask features at solution position can successfully identify the reliability of the solution.

TABLE V

RMS ERROR AND PERCENTAGE OF EPOCHS PASSED THE PROPOSED RULES FOR EXPERIMENT S2-Rx3 (METERS). WITHOUT IS ABBREVIATED AS W.O.

RMS (m)	w.o. rules	Rules combination									
		1	2	3	4	1+3	1+4	2+4	3+4	1+3+4	All rules
2D	17.30	17.30	12.08	17.07	17.30	17.07	17.30	12.08	17.07	17.07	12.15
Across	12.71	12.71	9.79	12.77	12.71	12.77	12.71	9.79	12.77	12.77	9.44
Along	11.74	11.74	7.08	11.33	11.74	11.33	11.74	7.08	11.33	11.33	7.65
Availability (%)		100.00	52.49	43.23	100.00	43.23	100.00	52.49	43.23	43.23	21.14

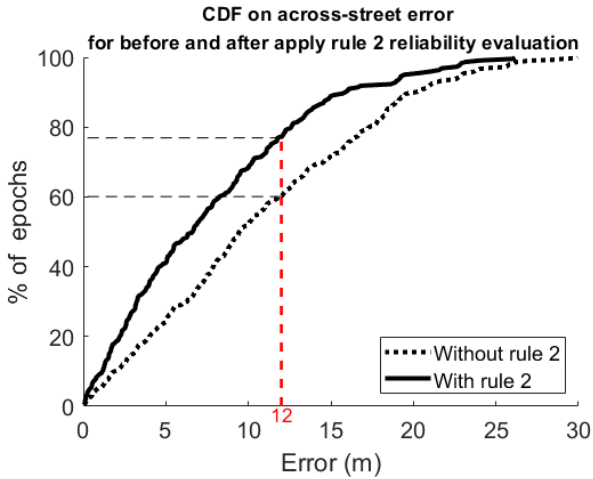


Fig. 14. Cumulative distribution function (CDF) of the positioning error on the across-street direction before and after epochs solution exclusion for S2-Rx3. The red dashed line represents the half street width of experiment S2-Rx3.

TABLE VI

RMS ERROR AND PERCENTAGE OF EPOCHS PASSED THE PROPOSED RULES FOR EXPERIMENT S3-Rx2 (METERS). WITHOUT IS ABBREVIATED AS W.O.

RMS (m)	w.o. rules	Rules combination									
		1	2	3	4	1+3	1+4	2+4	3+4	1+3+4	All rules
2D	40.25	40.25	16.05	34.36	40.29	34.36	40.29	16.08	34.40	34.40	16.22
Across	15.27	15.27	13.73	14.60	15.28	14.60	15.28	13.76	14.62	14.62	13.95
Along	37.24	37.24	8.30	31.10	37.28	31.10	37.28	8.32	31.14	31.14	8.27
Availability (%)		100.00	50.10	73.60	99.79	73.60	99.79	49.90	73.39	73.39	46.78

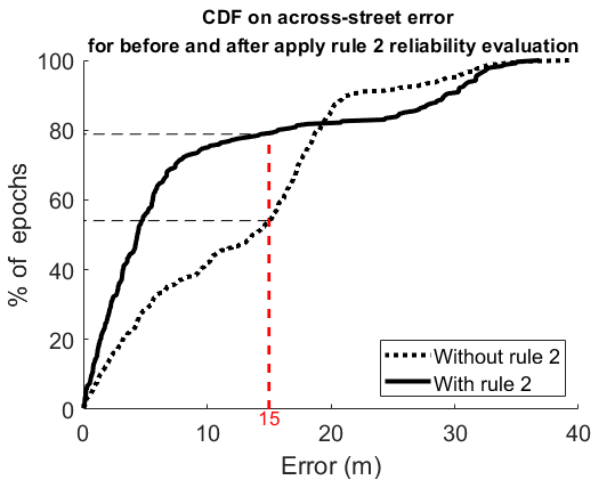


Fig. 15. CDF of the positioning error on across-street direction before and after epochs solution exclusion for S3-Rx2. The red dashed line represents the half street width of experiment S2-Rx3.

TABLE VII

RMS ERROR AND PERCENTAGE OF EPOCHS PASSED THE PROPOSED RULES FOR EXPERIMENT S4-Rx1 (METERS). WITHOUT IS ABBREVIATED AS W.O.

RMS (m)	w.o. rules	Rules combination									
		1	2	3	4	1+3	1+4	2+4	3+4	1+3+4	All rules
2D	17.76	17.76	6.89	17.65	17.76	17.65	17.76	6.89	17.65	17.65	6.89
Across	4.86	4.86	3.66	4.87	4.86	4.87	4.86	3.66	4.87	4.87	3.66
Along	17.08	17.08	5.84	16.96	17.08	16.96	17.08	5.84	16.96	16.96	5.84
Availability (%)		100.00	0.93	98.13	100.00	98.13	100.00	0.93	98.13	98.13	0.93

After the reliability test to exclude the epochs based on the Rule 2 criteria, about 77% of solutions is smaller than the half-width of the street, as shown in Fig. 14. The percentage of without reliability test of 60%. The result shows that the reliability test can increase the percentage of the solutions within half street width.

The experiment S3-Rx2 positioning results with reliability evaluation are shown in Table VI. As mention in section IV.B.2), the large positioning results due to the similarity on building structure at the opposite side of the street. With the evaluation factor exclusion, the positioning accuracy improves much. Especially rule 2 and other criteria with rule 2. Which means the rule 2 shows the key satellites cannot provide enough uniqueness to the building boundaries to match the optimal positioning candidate. After the reliability evaluation, 78.8% of valid solution across-street direction error is smaller than half street width, shown in Fig. 15.

The experiment S4-Rx1 reliability results are shown in Table VII. The results also show that Rule 2 can exclude those unreliable epochs and result in about 7m in 2D direction. And positioning error with 4m and 7m in across- and along-street directions, respectively. Most of the epochs were excluded by Rule 2, the ground truth for experiment S4 may be similar to other sample candidates, so it is hard to determine the exact user position accurately uniquely.

From the reliability test and exclusion results, the positioning improvement is larger when applying on smartphones. Due to the smartphone or other low-cost receivers, their design is to acquire and track as much signal as it can, in other words, the number of the NLOS reception will be increased. This increment will affect both the classification of intelligent classifier and the shadow matching positioning. However, with the reliability evaluation, the unreliable epoch solution can be excluded, improving the positioning accuracy and robustness.

V. CONCLUSION AND FUTURE WORKS

In this study, the shadow matching with intelligent classifier

and reliability test is introduced. The intelligent classifier is successfully classifying the NLOS reception and obtain a better shadow matching solution. With the intelligent classifier to improve the satellite visibility estimation, the across street direction can achieve within 10m error. Furthermore, the idea

of shadow matching reliability indicators and key satellite are introduced. The exclusion based on the proposed reliability test shows that shadow matching performance can be improved especially on the smartphone data where the quality of the measurements is relatively poor and noisy. Several experiment results show that the proposed Rule 2 on the key satellites matching with skymask can exclude the solution of epoch with large error. From this conclusion, it shows that the shadow matching needs good satellites distribution as well as enough skymask uniqueness for its matching.

The satellites at each candidate only score by the similarity of satellite visibility. This makes the resolution of the score limited, or the multiple clusters may easily occur if the high similarity of surrounding skymask. As a result, the scoring scheme may be re-designed by identifying the possible key satellite based on the received signal features. A higher weighting should be given to the matching with skymask. This idea should be able to improve the shadow matching results.

In conclusion, this paper defines a reliable solution of the GNSS shadow matching by passing the proposed rules used to exclude suspicious solutions (that are not fulfilling the rules of a good estimation of shadow matching.) However, we cannot guarantee that the proposed solutions fulfil any level of integrity.

REFERENCES

- [1] L. Chen *et al.*, "Robustness, Security and Privacy in Location-Based Services for Future IoT: A Survey," *IEEE Access*, vol. 5, pp. 8956-8977, 2017, doi: 10.1109/ACCESS.2017.2695525.
- [2] P. Dabove and M. G. Petovello, "What are the actual performances of GNSS positioning using smartphone technology?," *Inside GNSS*, vol. 9, pp. 34-37, 2014.
- [3] K. M. Pesyna, R. W. Heath, and T. E. Humphreys, "Centimeter Positioning with a Smartphone-Quality GNSS Antenna," in *Proceedings of the 27th International Technical Meeting of The Satellite Division of the Institute of Navigation (ION GNSS+ 2014)*, Tampa, Florida, September 2014 2014, pp. 1568-1577.
- [4] P. D. Groves, "Multipath vs. NLOS signals," *Inside GNSS*, vol. 8, pp. 40-42, 2013.
- [5] L.-T. Hsu, "Analysis and modeling GPS NLOS effect in highly urbanized area," *GPS Solutions*, vol. 22, no. 1, p. 7, 2018.
- [6] P. D. Groves and Z. Jiang, "Height Aiding, C/N0 Weighting and Consistency Checking for GNSS NLOS and Multipath Mitigation in Urban Areas," *Journal of Navigation*, vol. 66, no. 5, pp. 653-669, 2013, doi: 10.1017/S0373463313000350.
- [7] L.-T. Hsu, H. Tokura, N. Kubo, Y. Gu, and S. Kamijo, "Multiple Faulty GNSS Measurement Exclusion Based on Consistency Check in Urban Canyons," *IEEE Sensors Journal*, vol. 17, no. 6, pp. 1909-1917, 2017, doi: 10.1109/JSEN.2017.2654359.
- [8] J. Moreau, S. Ambellouis, and Y. Ruichek, "Fisheye-Based Method for GPS Localization Improvement in Unknown Semi-Obstructed Areas," *Sensors*, vol. 17, no. 1, p. 119, 2017, doi: 10.3390/s17010119.
- [9] T. Suzuki and N. Kubo, "N-LOS GNSS signal detection using fish-eye camera for vehicle navigation in urban environments," *27th International Technical Meeting of the Satellite Division of the Institute of Navigation, ION GNSS 2014*, vol. 3, pp. 1897-1906, 2014.
- [10] W. Wen, G. Zhang, and L. Hsu, "GNSS NLOS Exclusion Based on Dynamic Object Detection Using LiDAR Point Cloud," *IEEE Transactions on Intelligent Transportation Systems*, pp. 1-10, 2019, doi: 10.1109/TITS.2019.2961128.
- [11] W. Wen, G. Zhang, and L.-T. Hsu, "Correcting NLOS by 3D LiDAR and Building Height to improve GNSS Single Point Positioning," *NAVIGATION, Journal of the Institute of Navigation*, vol. 66, pp. 705-718, 2019, doi: 10.1002/navi.335.
- [12] X. Bai, W. Wen, G. Zhang, and L.-T. Hsu, "Real-time GNSS NLOS Detection and Correction Aided by Sky-Pointing Camera and 3D LiDAR," *Proceedings of the ION 2019 Pacific PNT Meeting*, pp. 862-874, April 2019 2019.
- [13] G. Sohn and I. Dowman, "Data fusion of high-resolution satellite imagery and LiDAR data for automatic building extraction," *ISPRS Journal of Photogrammetry and Remote Sensing*, vol. 62, no. 1, pp. 43-63, 2007, doi: 10.1016/j.isprsjprs.2007.01.001.
- [14] R. Wang, "3D building modeling using images and LiDAR: a review," *International Journal of Image and Data Fusion*, vol. 4, no. 4, pp. 273-292, 2013, doi: 10.1080/19479832.2013.811124.
- [15] P. D. Groves, "It's Time for 3D Mapping-Aided GNSS," *Inside GNSS Magazine*, 09/01 2016.
- [16] M. Obst, S. Bauer, and G. Wanielik, "Urban multipath detection and mitigation with dynamic 3D maps for reliable land vehicle localization," in *Proceedings of the 2012 IEEE/ION Position, Location and Navigation Symposium*, 23-26 April 2012 2012, pp. 685-691, doi: 10.1109/PLANS.2012.6236944.
- [17] L. Wang, P. D. Groves, and M. K. Ziebart, "GNSS Shadow Matching: Improving Urban Positioning Accuracy Using a 3D City Model with Optimized Visibility Scoring Scheme," *Navigation*, vol. 60, no. 3, pp. 195-207, 2013.
- [18] P. D. Groves, "Shadow Matching: A New GNSS Positioning Technique for Urban Canyons," *Journal of Navigation*, vol. 64, no. 3, pp. 417-430, Jul 2011, doi: 10.1017/S0373463311000087.
- [19] P. D. Groves, Q. Zhong, R. Faragher, and P. Esteves, "Combining Inertially-aided Extended Coherent Integration (Supercorrelation) with 3D-Mapping-Aided GNSS," *ION GNSS+ 2020*, 2020.
- [20] L.-T. Hsu, Y. Hu, and S. Kamijo, "3D building model-based pedestrian positioning method using GPS/GLONASS/QZSS and its reliability calculation," *GPS Solutions*, vol. 20, no. 3, pp. 413-428, 2016.
- [21] S. Miura, L.-T. Hsu, and F. Chen, "GPS Error Correction With Pseudorange Evaluation Using

Three-Dimensional Maps," *IEEE Transactions on Intelligent Transportation Systems*, vol. 16, no. 6, pp. 3104-3115, 2015.

- [22] H.-F. Ng, G. Zhang, and L.-T. Hsu, "A Computation Effective Range-based 3D Mapping Aided GNSS with NLOS Correction Method," *Journal of Navigation*, pp. 1-21, 2020.
- [23] L. Wang, P. D. Groves, and M. K. Ziebart, "Smartphone Shadow Matching for Better Cross-street GNSS Positioning in Urban Environments," *Journal of Navigation*, vol. 68, no. 3, pp. 411-433, 2015, doi: 10.1017/S0373463314000836.
- [24] R. Sun, L.-T. Hsu, D. Xue, G. Zhang, and W. Y. Ochieng, "GPS Signal Reception Classification Using Adaptive Neuro-Fuzzy Inference System," *Journal of Navigation*, vol. 72, no. 3, pp. 685-701, 2019, doi: 10.1017/S0373463318000899.
- [25] R. Yozevitch, B. B. Moshe, and A. Weissman, "A Robust GNSS LOS/NLOS Signal Classifier," *Navigation*, vol. 63, no. 4, pp. 429-442, 2016/12/01 2016, doi: 10.1002/navi.166.
- [26] B. Xu, Q. Jia, Y. Luo, and L. T. Hsu, "Intelligent GPS L1 LOS/multipath/NLOS classifiers based on correlator-, RINEX- and NMEA-level measurements," *Remote Sensing*, vol. 11, no. 16, p. 1851, 2019, doi: 10.3390/rs11161851.
- [27] (1995). *Explanatory Notes on Geodetic Datums in Hong Kong*.
- [28] G. Zhang, W. Wen, and L.-T. Hsu, "Rectification of GNSS-based collaborative positioning using 3D building models in urban areas," *GPS Solut*, vol. 23, no. 3, pp. 1-12, 2019, doi: 10.1007/s10291-019-0872-9.
- [29] L. Hsu, "GNSS multipath detection using a machine learning approach," in *2017 IEEE 20th International Conference on Intelligent Transportation Systems (ITSC)*, 16-19 Oct. 2017 2017, pp. 1-6, doi: 10.1109/ITSC.2017.8317700.
- [30] E. Realini and M. Reguzzoni, "Gogps: open source software for enhancing the accuracy of low-cost receivers by single-frequency relative kinematic positioning," *Measurement Science and technology*, vol. 24, no. 11, p. 115010, 2013, doi: 10.1088/0957-0233/24/11/115010.



GUOHAO ZHANG (S'19) received the bachelor's degree in mechanical engineering and automation from University of Science and Technology Beijing, China, in 2015. He received the master's degree in mechanical engineering and currently pursuing the Ph.D. degree in the Hong Kong Polytechnic University. His research interests including GNSS urban localization, cooperative positioning and multi-sensor integrated navigation.



LI-TA HSU (S'09-M'15) received the B.S. and Ph.D. degrees in aeronautics and astronautics from National Cheng Kung University, Taiwan, in 2007 and 2013, respectively. He is currently an assistant professor with the Division of Aeronautical and Aviation Engineering, Hong Kong Polytechnic University, before he served as post-doctoral researcher in Institute of Industrial Science at University of Tokyo, Japan. In 2012, he was a visiting scholar in University College London, U.K. He is an Associate Fellow of RIN.

His research interests include GNSS positioning in challenging environments and localization for pedestrian, autonomous driving vehicle and unmanned aerial vehicle.

HOI-FUNG NG received a Bachelor of Engineering (Honours) in Air Transport Engineering from The Hong Kong Polytechnic University, Hong Kong, in 2018. He is currently an M.Sc. student at the Department of Mechanical Engineering, The Hong Kong Polytechnic University, Hong Kong. His research interests including GNSS localization, navigation.

